PHYSICAL REVIEW B **103**, L201407 (2021)

Letter

Nonequilibrium phonon tuning and mapping in few-layer graphene with infrared nanoscopy

Jun Qian,[1,2,3] Yilong Luan,[1,2] Minsung Kim,[1,2] Kai-Ming Ho,[1,2] Yi Shi,[3] Cai-Zhuang Wang,[1,2,*]
Yun Li,[3,†] and Zhe Fei[1,2,‡]
[1]*Department of Physics and Astronomy, Iowa State University, Ames, Iowa 50011, USA*
[2]*Ames Laboratory, U. S. Department of Energy, Iowa State University, Ames, Iowa 5001 1, USA*
[3]*National Laboratory of Solid-State Microstructures, School of Electronic Science and Engineering,*
Collaborative Innovation Center of Advanced Microstructures, Nanjing University, Nanjing 210093, People's Republic of China

(Received 1 March 2020; revised 4 May 2021; accepted 5 May 2021; published 27 May 2021; corrected 7 March 2022)

Electron-phonon interactions are fundamentally important physical processes responsible for many key discoveries in condensed matter physics and material sciences. Herein, by exploiting the scattering-type scanning near-field optical microscope (s-SNOM) excited with a femtosecond infrared (IR) laser, we explored the strong coupling between IR phonons in few-layer graphene (FLG) with ultrahot electrons, which are heated up by the intense laser field enhanced by the s-SNOM tip. More specifically, we found that the intensity of the phonon resonance can be tuned systematically by varying the laser power that controls the electron temperature. Furthermore, the high spatial resolution of s-SNOM allows us to map the local phonon characteristics at sharp boundaries and nanostructures. Our findings offer insights into the intriguing physics behind the electron-phonon interactions in nonequilibrium conditions and open a pathway for manipulating phonons with optical means.

DOI: 10.1103/PhysRevB.103.L201407

In recent years, graphene and its thicker counterparts have attracted tremendous research interest owing to their superior properties [1–3], which profoundly promote both fundamental sciences and technological applications [4–7]. Nearly all the electronic, optical, and thermal properties of these materials are closely related to the responses of electrons, phonons, and their coherent interactions. Indeed, electron-phonon interactions are responsible for many peculiar physical phenomena in graphene and few-layer graphene (FLG), such as Fermi-velocity renormalization [8,9], giant tunneling conductance [10], magnetophonon oscillations [11,12], and unconventional superconductivity [13,14]. These fascinating phenomena have therefore inspired further studies of graphene phonons and their coupling with electronic excitations in the two-dimensional (2D) flatland.

Infrared (IR) spectroscopy has been proven to be a powerful tool in probing optical phonons in FLG (i.e., two layers and above) [15–18], but not in single-layer graphene (SLG) due to the lack of net dipole moments. There are many unique phenomena related to IR phonons in FLG, among which the "charged-phonon" effect attracts a lot of research interest [15–22]. This effect originates from the coupling between IR phonons with interband electronic excitations in FLG, resulting in interesting gate-tunable phonon anomalies. So far, the studies of IR phonons of FLG and their interactions with electrons were performed mainly by far-field spectroscopy that typically has a low excitation power due to the usage of weak IR sources (e.g., Globar). Therefore, IR phonons are coupled with relatively cold electrons at equilibrium conditions. Responses of graphene phonons interacting with nonequilibrium hot electrons remain largely unexplored.

In this Letter, we report a nano-IR spectroscopy study of phonon responses in FLG using the scattering-type scanning near-field optical microscope (s-SNOM) that is built on an atomic force microscope (AFM) (see the Supplemental Material [23]). By coupling s-SNOM with a broadband femtosecond (fs) laser, we were able to perform IR spectroscopy with a high spatial resolution (∼20 nm), which is convenient for probing and mapping small graphene microcrystals and nanostructures. The spectral window of the laser is selected to be 1100–1900 cm^{-1} (corresponding to 0.14–0.24 eV) that covers the graphene phonon resonance (∼0.2 eV). The fs laser has a pulse width of ∼100 fs and average power up to 1 mW. With further enhancement by the conductive s-SNOM tip, electrons can be heated up to very high temperatures [23,24] and strongly impact the phonon resonance of FLG. Note that the laser intensity is orders of magnitude lower than the saturation density reported in previous literature [25] due to the broadband nature of the laser pulses (1100 to 1900 cm^{-1}).

Our nano-IR setup is illustrated in Fig. 1(a), where the laser pulses are focused at the apex of the s-SNOM tip. The tip-scattered pulses, which are partially collected by the detector, contain key nano-IR signals of the sample right underneath the tip. By implementing a Michelson interferometer setup (Fig. S1 [23]), we can extract both the amplitude and phase of the nano-IR signals. We discuss in the main text the amplitude (s) signal that is ideal for revealing phonon resonances [26,27]. The phase data are consistent with the amplitude and are discussed in the Supplemental Material [23]. Our samples were fabricated by mechanical exfoliations of bulk graphite onto the standard SiO_2/Si substrates. The thicknesses and stacking orders of graphene samples were determined by a

---

[*] Corresponding author: wangcz@iastate.edu
[†] Corresponding author: yli@nju.edu.cn
[‡] Corresponding author: zfei@iastate.edu

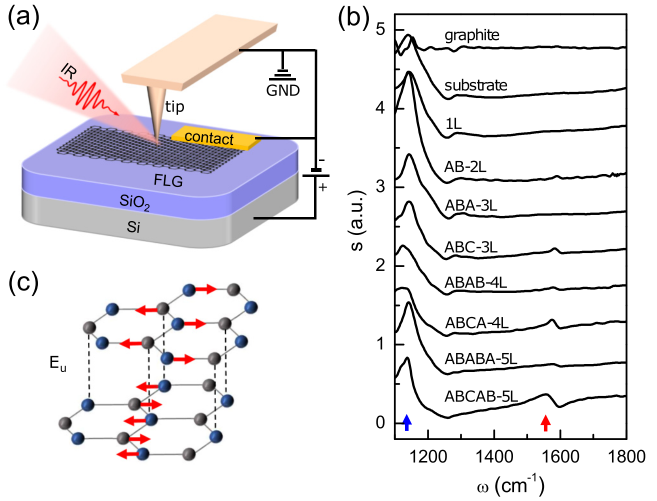

FIG. 1. (a) Illustration of the s-SNOM study of FLG excited by an fs IR beam. (b) The nano-IR spectra of the substrate, graphite, and graphene layer(s) with different thicknesses and stacking orders. Here we use 1L, 2L, … to label the thickness, and use AB, ABA, ABC, etc., to label the stacking order. The spectra are displaced vertically for clarity. The blue and red arrows mark the SiO$_2$ and graphene phonons, respectively. (c) Sketch of the atomic displacements of the IR-active E_u phonon in bilayer graphene as indicated by the arrow directions.

combination of optical microscopy, AFM, and s-SNOM imaging (Fig. S2). Throughout the Letter, we label the thickness of single-layer to pentalayer graphene as "1L" to "5L," respectively. For stacking orders, we use "AB," "ABA," etc., for Bernal stacking and "ABC," "ABCA," etc., for rhombohedral stacking.

In Fig. 1(b), we plot the nano-IR amplitude spectra $s(\omega)$ of graphene/graphite samples with various thicknesses and stacking orders. Here graphene samples were electrically doped by gating. All IR spectra were normalized to that of gold and displaced vertically for clarity. Gold is a standard reference material in IR due to the overall flat response. As shown in Fig. 1(b), there is one dominant resonance at $\sim$1130 cm^{-1} (blue arrow) in the spectra, which is attributed to the optical phonon of SiO$_2$ [26,27]. Besides, there is a weaker resonance feature centered at $\sim$1580 cm^{-1} (red arrow) in nearly all samples except SLG, ABA-3L graphene, and graphite, which originates from the IR-active E_u or E' phonons [Fig. 1(c)] [15,22,28]. The IR phonon does exist in ABA-3L graphene and graphite, according to far-field studies [18,22], but they are too weak to be resolved by s-SNOM. Clearly, both the intensity and shape of phonon resonances are different from sample to sample. As reported previously [15,17,18], the observed thickness and stacking dependences of phonon resonances of FLG are directly linked to the coherent electron-phonon interactions. In this work, we focus on ABC-3L graphene for quantitative analysis of the hot-electron responses. Other FLG samples share similar responses and are discussed in the Supplemental Material [23].

We first performed nano-IR spectroscopy of FLG by tuning its carrier density with back gating. As an example, we plot in Fig. 2(a) gate-tunable IR spectra $s(\omega)$ of ABC-3L graphene. Here we label the difference between the gate voltage (V_g) and the charge-neutral voltage (V_{CN}), namely V_g-V_{CN}, which is proportional to the carrier density. We mainly focus on the hole doping side (V_g-$V_{CN} < 0$) in the current work. The responses of phonon resonances on the electron doping side are expected to be similar according to previous studies [15,18]. In all gating measurements, we used a low laser power ($\sim$78 μW) that has relatively small heating on electrons. Clearly from Fig. 2(a), the phonon resonance demonstrates a systematic dependence with doping, which is a direct evidence of electron-phonon coupling. Gate-tunable IR phonons were also observed in other types of FLG (Fig. S3). Detailed discussions about gate-tunable phonons of FLG could be found in previous far-field studies [15,16,18].

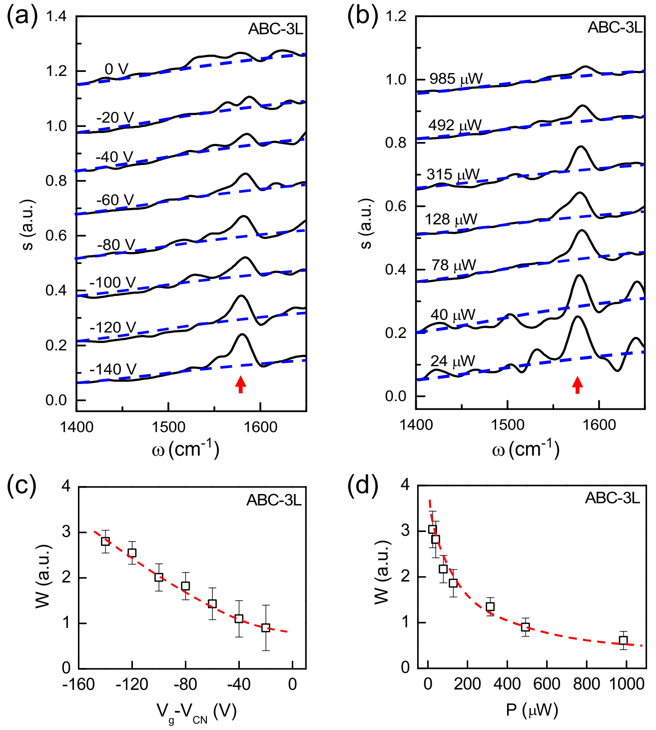

FIG. 2. (a) Nano-IR spectra revealing gate-tunable phonon resonance in ABC-3L graphene. The average power is set to be 78 μW. The labeled voltages are V_g-V_{CN}, namely the difference between the gate voltage (V_g) and the charge neutrality point (V_{CN}). (b) Power-dependent nano-IR spectra of ABC-3L graphene with V_g-$V_{CN} = -80$ V. The blue dashed curves in (a) and (b) mark the background signal. (c), (d) The phonon intensity W versus V_g-V_{CN} and laser power, which were extracted from (a) and (b), respectively. The red dashed curves here are drawn to guide the eye.

While gating tunes the carrier density, varying the laser power (P) can effectively control the electron temperature (T_e) of graphene [24,29–31]. In Fig. 2(b), we plot the P-dependent nano-IR spectra of hole-doped ABC-3L graphene (V_g-$V_{CN} = -80$ V), where one can see that the phonon resonance shrinks systematically with increasing P. Following Ref. [15], we fit the background-subtracted phonon resonances with the Fano formula $\Delta s(\omega) = (W/\Gamma)\{(q^2 + 2qz - 1)/[q^2(1 + z^2)]\}$ with $z = 2(\omega - \omega_0)/\Gamma$. Here W describes the phonon intensity, ω_0 is the resonance frequency, Γ is the linewidth,

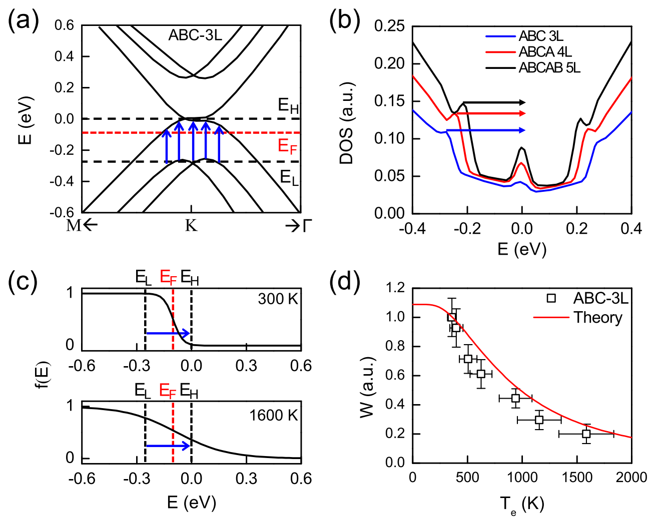

FIG. 3. (a) The band structure of ABC-3L graphene obtained with first-principle calculations [23]. The red and black dashed lines marked the estimated E_F ($\sim -0.08\,\mathrm{eV}$) and the low (E_L) and high (E_H) energies associated with the key interband transitions (arrows). (b) The calculated DOS of various FLG samples. (c) The Fermi-Dirac distribution for $T_e = 300$ and 1600 K, respectively. (d) Experimental and calculated phonon intensity $W(T_e)$ of ABC-3L graphene, normalized to W at $P = 24\,\mu\mathrm{W}$ and $T_e = 358\,\mathrm{K}$, respectively.

and q is the dimensionless parameter that describes Fano asymmetry. We discuss mainly the responses of W here, and the effects of other parameters are less prominent and are introduced in the Supplemental Material [23]. The extracted W of ABC-3L graphene is plotted in Figs. 2(c) and 2(d), where one can see that W can be controlled effectively by tuning both V_g and P. More interestingly, the power dependence of W appears to be exponential while the gate dependence is approximately linear. Power-dependence measurements have also been performed in other FLG samples (Fig. S4). In all cases, exponential decay of the phonon intensity with increasing P has been observed.

Before discussing the power-dependent responses, we first briefly describe electron-phonon interactions for cold electrons at equilibrium conditions. According to previous studies [15–21], the interactions are mainly due to the coupling between the phonon resonance and interband transitions. More specifically, the strong interband resonance can transfer oscillator strength to the phonon resonance, thus significantly enhancing the latter. The interband transitions are also responsible for other interesting responses (e.g., Fano asymmetry and phonon softening) of the phonon resonance (see Ref. [15] and Supplemental Material [23]). Among all possible interband transitions, the most relevant ones to the phonon intensity are between the high- (low-)lying valence (conduction) bands in the case of hole (electron) doping. We sketched in Fig. 3(a) these interband transitions (blue arrows) on the band structure of hole-doping ABC-3L graphene. The relatively flat bands close to the maxima of the valence bands (marked with E_H and E_L) result in high densities of states (DOS) [Fig. 3(b)] and hence strong interband transitions. The band structures and DOS shown in this work were obtained with first-principles calculations using a number of density-functional-theory techniques [32] (see Supplemental Material [23]). From Fig. 3(a), one can see that more states are available for interband transitions at higher doping levels, which accounts for the observed gate dependence of phonon resonances in Fig. 2(a) [15,18]. For FLG with different thicknesses and stacking orders, the energy and intensity of the interband resonance vary from one to another [33], resulting in their unique phonon resonances and responses [see Fig. 1(b) and Refs. [15,17,18]]. The hump-shaped interband resonance of the ABCAB-5L graphene with a linewidth of $\sim 500\,\mathrm{cm}^{-1}$ and a peak frequency of $\sim 1800\,\mathrm{cm}^{-1}$ (black arrow) can be seen in our nano-IR spectra (Figs. S3 and S4). In the case of other FLG samples, the peak energies of the interband resonance are higher [33] and out of the experimental range [see Figs. 3(b) and S11].

When exciting graphene with tip-enhanced fs pulses, electrons can be heated up significantly. The heating is initiated by the absorption of broadband IR photons through both interband and intraband transitions. After an extremely fast carrier thermalization (<30 fs) [24,30,31], carriers are characterized by a single Fermi-Dirac distribution with an effective T_e. To estimate T_e, we performed finite-element simulations considering tip-enhanced pulse heating, thermal conduction [34], and electron-phonon heat transfer. Detailed discussions about the simulations are given in the Supplemental Material [23]. According to the simulations, the average T_e of ABC-3L graphene underneath the tip scales monotonically with laser power, and it can reach up to 1600 K at full laser power [Fig. S12(d)]. Electrons do transfer heat to optical phonons close to K and Γ points [Fig. S12(b)], but the entire lattice remains relatively cold, so the system is in a nonequilibrium state within the pulse duration [29,35].

The most obvious effect of hot electrons is the thermal broadening of the Fermi surface, which strongly affects the interband transitions responsible for phonon enhancement. To demonstrate that, we plot in Fig. 3(c) the electron occupation at both room temperature ($T_e = 300\,\mathrm{K}$) and a high temperature ($T_e = 1600\,\mathrm{K}$) based on the Fermi-Dirac function $f(E) = \{\exp[(E\text{-}E_F)/kT_e] + 1\}^{-1}$, where k is Boltzmann's constant. We mark in Fig. 3(c) the relevant low (E_L) and high (E_H) energies for the key interband transitions sketched in Fig. 3(a). The Fermi energy (E_F) is estimated to be about -0.08 eV for ABC-3L graphene with V_g-$V_{CN} = -80\,\mathrm{V}$ (hole doping), so E_F is sandwiched by E_L and E_H. At $T_e \approx 300\,\mathrm{K}$, electron states are almost fully occupied at E_L and unoccupied at E_H, so interband transitions from E_L to E_H are largely unaffected. At $T_e = 1600\,\mathrm{K}$, states at both E_L and E_H are partially occupied, so interband transitions will be suppressed.

For quantitative discussions, we refer to the charged-phonon theory of FLG introduced previously [20,21]. According to the theory, the phonon intensity W of FLG is proportional to $[\mathrm{Re}(\chi)]^2$, where χ is the mixed current-phonon response function and can be obtained by summating $[f(E_i) - f(E_f)]/[\hbar\omega_0\text{–}(E_f\text{–}E_i) + i\eta]$ over all the states for the relevant interband transitions. Here E_i and E_f are the energies for the initial and final states of the transition, $\hbar\omega_0 \approx 0.2\,\mathrm{eV}$ is the phonon energy, and η is the broadening parameter of interband transitions [21]. We set η to be 0.01 eV following a previous far-field study of ABC-3L graphene [36].

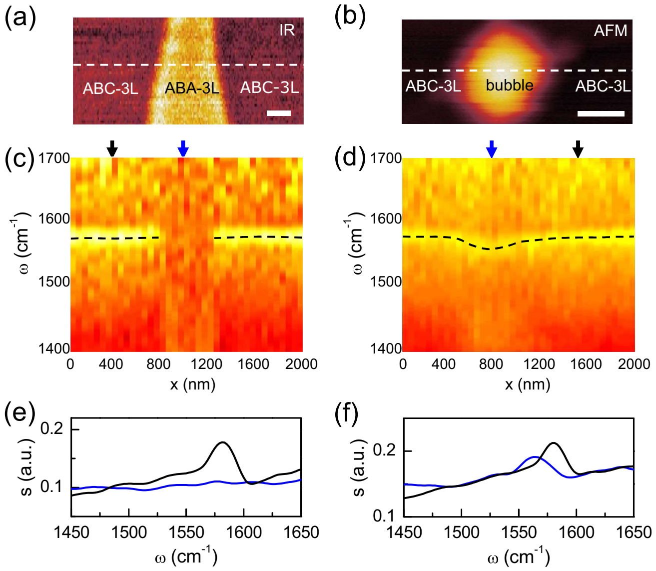

FIG. 4. (a) The nano-IR amplitude image of an ABC/ABA/ABC-3L graphene junction. (b) The AFM topography image revealing a nanobubble in ABC-3L graphene. The scales bars represent 200 nm. (c), (d) Hyperspectral maps that were taken along the white dashed lines in (a) and (b), respectively. The horizontal and vertical axes correspond to tip location (x) and IR frequency (ω), respectively. The black dashed lines mark the peak frequency of the phonon resonance. (d)–(f) The nano-IR spectra extracted from the hyperspectral maps at locations marked by the arrows in (c) and (d).

If considering only the key interband transitions sketched in Fig. 3(a) for approximation, W has the following relationship:

$$W(T_e) \approx A\left\{\mathrm{Re}\left[\frac{f(E_L)-f(E_H)}{\hbar\omega_0-(E_H-E_L)+i\eta}\right]\right\}^2, \qquad (1)$$

where A is a T_e-independent coefficient. Based on Eq. (1), we plot in Fig. 3(d) the normalized $W(T_e)$ curve of ABC-3L, where one can see that W drops systematically as T_e increases. The decay is exponential due to the factor $f(E_L)$-$f(E_H)$, which accounts for the thermal broadening picture described above [Fig. 3(c)]. In Fig. 3(d), we also add the experimental data points of ABC-3L graphene after converting laser power into T_e based on the calculated P-T_e dependence curve [Fig. S12(d)]. The general trend of the theory curve matches that of the experimental data points. For more accurate calculations, one needs to consider all possible interband transitions and the temperature dependence of η.

Finally, we took advantage of the high-resolution capability of the s-SNOM to probe the nano-IR phonon characteristics of FLG. In Fig. 4, we present the results taken at two representative sample regions: an ABC/ABA/ABC-3L graphene junction and an ABC-3L graphene nanobubble. The nanobubble here is formed when air, water, or hydrocarbons are trapped underneath the sample during the sample fabrication process [37–39]. In Figs. 4(a) and 4(b), we plot the s-SNOM and AFM images to reveal the local structure and geometry of the two sample regions. The nano-IR signal shown in the s-SNOM image [Fig. 4(a)] is integrated over the spectral range 1100–1900 cm^{-1}. Figures 4(c) and 4(d) are hyperspectral maps with horizontal and vertical axes corresponding to the tip location (x) and IR frequency ω, respectively. Each hyperspectral map consists of 40 nano-IR spectra taken as tip scans step by step (step size = 25 nm) along the white dashed lines in Figs. 4(a) and 4(b). We plot two representative spectra from each sample in Figs. 4(e) and 4(f), which correspond to the vertical line cuts at marked locations (arrows) in the hyperspectral maps [Figs. 4(c) and 4(d)].

The dominant feature in the hyperspectral images [Figs. 4(c) and 4(d)] is the bright IR phonon line close to $\omega = 1580\,\mathrm{cm}^{-1}$ in ABC-3L graphene (marked with dashed lines). The phonon line is not seen inside ABA-3L graphene due to the extremely weak intensity as discovered earlier [17,18]. The sharp cutoff of the phonon line at the ABC-ABA boundary proves the high resolution (∼25 nm) of our technique, which is required to probe small nanostructures. The ABC-3L graphene bubble shown in Fig. 4(b) is one such nanostructure. The diameter of the bubble is ∼200 nm with a height of ∼33 nm. Interestingly, we found that the phonon line curved downward in the bubble region. At the bubble center, the phonon frequency is $\sim 1565\,\mathrm{cm}^{-1}$, $16\,\mathrm{cm}^{-1}$ lower than that of the flat sample region ($\sim 1581\,\mathrm{cm}^{-1}$) [Fig. 4(f)]. The phonon softening is mainly due to the increase of tensile strain in the bubble region, which has been reported in previous Raman spectroscopy studies [40,41]. Nevertheless, the spatial resolution of far-field Raman spectroscopy is typically above 300 nm, which is not enough to resolve local strain distributions in small nanobubbles. In addition to phonon frequency, phonon intensity also drops significantly (by ∼30% at the bubble center), which is partly due to the shift of the phonon frequency away from the interband resonance and partly due to the decrease of doping when the sample is away from the substrate [42]. The change of doping ($< 5.8 \times 10^{12}\,\mathrm{cm}^{-2}$) also contributes slightly to the phonon softening, but it is estimated to be within $2\,\mathrm{cm}^{-1}$ [18].

In summary, we have performed a comprehensive nano-IR spectroscopy study of the intrinsic phonons in FLG using s-SNOM excited with a broadband fs laser. We demonstrated that our nano-IR spectroscopy with a nanoscale resolution is convenient for probing and mapping the local phonon characteristics in FLG microcrystals and nanostructures. Moreover, we found that the IR phonon intensity decreases systematically with increasing laser power, which is attributed to the strong coupling between phonons and nonequilibrium hot electrons excited by the laser. Quantitative analyses and simulations indicate that the average T_e of electrons, which is tunable by controlling the power, can reach up to 1600 K and can thus significantly quench the interband transitions and hence the phonon resonance. Our work deepens the understanding of nonequilibrium electron-phonon interactions in FLG and paves the way for future studies in a wide variety of quantum systems (e.g., unconventional superconductors [43,44], Weyl semimetals [45], perovskite semiconductors [46], semiconductor quantum dots [47], etc.), where electron-phonon coupling plays an essential role. Unlike electrical gating that is only effective in 2D materials, tuning T_e with power control can be applied in materials of all dimensions.

Work done at Ames Laboratory was supported by the U.S. Department of Energy, Office of Basic Energy Science, Division of Materials Sciences and Engineering. Ames Laboratory is operated for the U.S. Department of Energy by Iowa State University under Contract No. DE-AC02-07CH11358. The sample preparation was supported by the National Science Foundation under Grant No. DMR-1945560. J.Q. is thankful to the China Scholarship Council (CSC) for financial support. Y.L. acknowledges the funding support from Natural Science Foundation of Jiangsu Grant No. BK20170075, and National Natural Science Foundation of China Grants No. 61774080 and No. 61574074.

J.Q. and Y.L. contributed equally to this work.

---

[1] A. H. Castro Neto, F. Guinea, N. M. R. Peres, K. S. Novoselov, and A. K. Geim, Rev. Mod. Phys. **81**, 109 (2009).

[2] S. Das Sarma, S. Adam, E. H. Hwang, and E. Rossi, Rev. Mod. Phys. **83**, 407 (2011).

[3] D. N. Basov, M. M. Fogler, A. Lanzara, F. Wang, and Y. Zhang, Rev. Mod. Phys. **86**, 959 (2014).

[4] F. Bonaccorso, Z. Sun, T. Hasan, and A. C. Ferrari, Nat. Photonics **4**, 611 (2010).

[5] F. Bonaccorso, L. Colombo, G. Yu, M. Stoller, V. Tozzini, A. C. Ferrari, R. S. Ruoff, and V. Pellegrini, Science **347**, 1246501 (2015).

[6] T. Low and P. Avouris, ACS Nano **8**, 1086 (2014).

[7] W. Han, R. K. Kawakami, M. Gmitra, and J. Fabian, Nat. Nanotechnol. **9**, 794 (2014).

[8] W.-K. Tse and S. Das Sarma, Phys. Rev. Lett. **99**, 236802 (2007).

[9] C.-H. Park, F. Giustino, M. L. Cohen, and S. G. Louie, Nano Lett. **8**, 4229 (2008).

[10] Y. Zhang, V. W. Brar, F. Wang, C. Girit, Y. Yayon, M. Panlasigui, A. Zettl, and M. F. Crommie, Nat. Phys. **4**, 627 (2008).

[11] P. Kumaravadivel, M. T. Greenaway, D. Perello, A. Berdyugin, J. Birkbeck, J. Wengraf, S. Liu, J. H. Edgar, A. K. Geim, L. Eaves *et al.*, Nat. Commun. **10**, 3334 (2019).

[12] C. Cong, J. Jung, B. Cao, C. Qiu, X. Shen, A. Ferreira, S. Adam, and T. Yu, Phys. Rev. B **91**, 235403 (2015).

[13] Y. Cao, V. Fatemi, S. Fang, K. Watanabe, T. Taniguchi, E. Kaxiras, and P. Jarillo-Herrero, Nature (London) **556**, 43 (2018).

[14] B. Lian, Z. Wang, and B. A. Bernevig, Phys. Rev. Lett. **122**, 257002 (2019).

[15] A. B. Kuzmenko, L. Benfatto, E. Cappelluti, I. Crassee, D. van der Marel, P. Blake, K. S. Novoselov, and A. K. Geim, Phys. Rev. Lett. **103**, 116804 (2009).

[16] T.-T. Tang, Y. Zhang, C.-H. Park, B. Geng, C. Girit, Z. Hao, M. C. Martin, A. Zettl, M. F. Crommie, S. G. Louie, Y. R. Shen, and F. Wang, Nat. Nanotechnol. **5**, 32 (2010).

[17] Z. Li, C. H. Lui, E. Cappelluti, L. Benfatto, K. F. Mak, G. L. Carr, J. Shan, and T. F. Heinz, Phys. Rev. Lett. **108**, 156801 (2012).

[18] C. H. Lui, E. Cappelluti, Z. Li, and T. F. Heinz, Phys. Rev. Lett. **110**, 185504 (2013).

[19] T. Ando, J. Phys. Soc. Jpn. **76**, 104711 (2007).

[20] E. Cappelluti, L. Benfatto, and A. B. Kuzmenko, Phys. Rev. B **82**, 041402(R) (2010).

[21] E. Cappelluti, L. Benfatto, M. Manzardo, and A. B. Kuzmenko, Phys. Rev. B **86**, 115439 (2012).

[22] M. Manzardo, E. Cappelluti, E. van Heumen, and A. B. Kuzmenko, Phys. Rev. B **86**, 054302 (2012).

[23] See Supplemental Material at http://link.aps.org/supplemental/10.1103/PhysRevB.103.L201407 for additional experimental and theoretical details and results.

[24] M. Wagner, Z. Fei, A. S. McLeod, A. S. Rodin, W. Bao, E. G. Iwinski, Z. Zhao, M. Goldflam, M. Liu, G. Dominguez *et al.*, Nano Lett. **14**, 894 (2014).

[25] Q. Bao, H. Zhang, Y. Wang, Z. Ni, Y. Yan, Z. X. Shen, K. P. Loh, and D. Y. Tang, Adv. Funct. Mater. **19**, 3077 (2009); F. Zhang, S. Han, Y. Liu, Z. Wang, and X. Xu, Appl. Phys. Lett. **106**, 091102 (2015).

[26] Z. Fei, G. O. Andreev, W. Bao, L. M. Zhang, A. S. McLeod, C. Wang, M. K. Stewart, Z. Zhao, G. Dominguez, M. Thiemens *et al.*, Nano Lett. **11**, 4701 (2011).

[27] L. M. Zhang, G. O. Andreev, Z. Fei, A. S. McLeod, G. Dominguez, M. Thiemens, A. H. Castro-Neto, D. N. Basov, and M. M. Fogler, Phys. Rev. B **85**, 075419 (2012).

[28] J.-A. Yan, W. Y. Ruan, and M. Y. Chou, Phys. Rev. B **77**, 125401 (2008).

[29] C. H. Lui, K. F. Mak, J. Shan, and T. F. Heinz, Phys. Rev. Lett. **105**, 127404 (2010).

[30] D. Brida, A. Tomadin, C. Manzoni, Y. J. Kim, A. Lombardo, S. Milana, R. R. Nair, K. S. Novoselov, A. C. Ferrari, G. Cerullo *et al.*, Nat. Commun. **4**, 1987 (2013).

[31] Q. Ma, T. I. Andersen, N. L. Nair, N. M. Gabor, M. Massicotte, C. H. Lui, A. F. Young, W. Fang, K. Watanabe, T. Taniguchi *et al.*, Nat. Phys. **12**, 455 (2016).

[32] G. Kresse and J. Hafner, Phys. Rev. B **47**, 558 (1993); G. Kresse and J. Furthmüller, *ibid.* **54**, 11169 (1996); J. P. Perdew, K. Burke, and M. Ernzerhof, Phys. Rev. Lett. **77**, 3865 (1996); P. E. Blöchl, Phys. Rev. B **50**, 17953 (1994); S. Grimme, J. Antony, S. Ehrlich, and H. Krieg, J. Chem. Phys. **132**, 154104 (2010).

[33] D. S. Ki, H. Kwon, A. Y. Nikitin, S. Ahn, L. Martin-Moreno, F. J. Garcia-Vidal, S. Ryu, H. Min, and Z. H. Kim, ACS Nano **9**, 6765 (2015).

[34] T. Y. Kim, C.-H. Park, and N. Marzari, Nano Lett. **16**, 2439 (2016).

[35] J.-A. Yang, S. Parham, D. Dessau, and Dmitry Reznik, Sci. Rep. **7**, 40876 (2016).

[36] C. H. Lui, Z. Li, K. F. Mak, E. Cappelluti, and T. F. Heinz, Nat. Phys. **7**, 944 (2011).

[37] S. J. Haigh, A. Gholinia, R. Jalil, S. Romani, L. Britnell, D. C. Elias, K. S. Novoselov, L. A. Ponomarenko, A. K. Geim, and R. Gorbachev, Nat. Mater. **11**, 764 (2012).

[38] E. Khestanova, F. Guinea, L. Fumagalli, A. K. Geim, and I. V. Grigorieva, Nat. Commun. **7**, 12587 (2016).

[39] Z. Fei, J. J. Foley, W. Gannett, K. K. Liu, S. Dai, G. X. Ni, A. Zettl, M. M. Fogler, G. P. Wiederrecht, S. K. Gray, and D. N. Basov, Nano Lett. **16**, 7842 (2016).

[40] J. Zabel, R. R. Nair, A. Ott, T. Georgiou, A. K. Geim, A. S. Novoselov, and C. Casiraghi, Nano Lett. **12**, 617 (2012).

[41] D. Metten, F. Federspiel, M. Romeo, and S. Berciaud, Phys. Rev. Applied **2**, 054008 (2014).

[42] S. Ryu, L. Liu, S. Berciaud, Y.-J. Yu, H. Liu, P. Kim, G. W. Flynn, and L. E. Brus, Nano Lett. **10**, 4944 (2010).

[43] W. Weber, Phys. Rev. Lett. **58**, 1371 (1987).

[44] T. Timusk, C. D. Porter, and D. B. Tanner, Phys. Rev. Lett. **66**, 663 (1991).

[45] B. Xu, Y. M. Dai, L. X. Zhao, L. X. Zhao, K. Wang, R. Yang, W. Zhang, J. Y. Liu, H. Xiao, G. F. Chen, S. A. Trugman, J.-X. Zhu, A. J. Taylor, D. A. Yarotski, R. P. Prasankumar, and X. G. Qiu, Nat. Commun. **8**, 14933 (2017).

[46] X. Gong, O. Voznyy, A. Jain, W. Liu, R. Sabatini, Z. Piontkowski, G. Walters, G. Bappi, S. Nokhrin, O. Bushuyev *et al.*, Nat. Mater. **17**, 550 (2018).

[47] S. Hameau, Y. Guldner, O. Verzelen, R. Ferreira, G. Bastard, J. Zeman, A. Lemaitre, and J. M. Gerard, Phys. Rev. Lett. **83**, 4152 (1999).

Correction: The NSF support statement in the Acknowledgment section contained an error and has been fixed.